AGU PUBLICATIONS

Geophysical Research Letters

RESEARCH LETTER
10.1002/2017GL073163

Key Points:
- First results from electron MHD-based reconstruction of the electron diffusion region of magnetopause reconnection seen by MMS
- The X point was likely within a few kilometers of the MMS4 spacecraft but outside the MMS tetrahedron at the closest approach
- The estimated reconnection electric field is 0.42–0.98 mV/m, equivalent to the dimensionless reconnection rate of 0.11–0.25

Supporting Information:
- Supporting Information S1

Correspondence to:
H. Hasegawa
hase@stp.isas.jaxa.jp

Citation:
Hasegawa, H., et al. (2017), Reconstruction of the electron diffusion region observed by the Magnetospheric Multiscale spacecraft: First results, *Geophys. Res. Lett.*, *44*, 4566–4574, doi:10.1002/2017GL073163.

Received 19 FEB 2017
Accepted 9 MAY 2017
Accepted article online 11 MAY 2017
Published online 29 MAY 2017

Reconstruction of the electron diffusion region observed by the Magnetospheric Multiscale spacecraft: First results

H. Hasegawa[1], B. U. Ö. Sonnerup[2], R. E. Denton[3], T.-D. Phan[4], T. K. M. Nakamura[5], B. L. Giles[6], D. J. Gershman[6,7], J. C. Dorelli[6], J. L. Burch[8], R. B. Torbert[9], C. T. Russell[10], R. J. Strangeway[10], P.-A. Lindqvist[11], Y. V. Khotyaintsev[12], R. E. Ergun[13], P. A. Cassak[14], N. Kitamura[1], and Y. Saito[1]

[1]Institute of Space and Astronautical Science, Japan Aerospace Exploration Agency, Sagamihara, Japan, [2]Thayer School of Engineering, Dartmouth College, Hanover, New Hampshire, USA, [3]Department of Physics and Astronomy, Dartmouth College, Hanover, New Hampshire, USA, [4]Space Sciences Laboratory, University of California, Berkeley, California, USA, [5]Space Research Institute, Austrian Academy of Sciences, Graz, Austria, [6]NASA Goddard Space Flight Center, Greenbelt, Maryland, USA, [7]Oak Ridge Associated Universities, Washington, District of Columbia, USA, [8]Southwest Research Institute, San Antonio, Texas, USA, [9]Physics Department and Space Science Center, University of New Hampshire, Durham, New Hampshire, USA, [10]Department of Earth, Planetary, and Space Sciences, University of California, Los Angeles, California, USA, [11]Royal Institute of Technology, Stockholm, Sweden, [12]Swedish Institute of Space Physics, Uppsala, Sweden, [13]Department of Astrophysical and Planetary Sciences, University of Colorado Boulder, Boulder, Colorado, USA, [14]Department of Physics and Astronomy, West Virginia University, Morgantown, West Virginia, USA

Abstract We present first results of the reconstruction of the electron diffusion region (EDR) based on a two-dimensional, incompressible, and inertialess version of the electron magnetohydrodynamics equations. The method is applied to 30 ms resolution magnetic field, and electron moments data taken when the Magnetospheric Multiscale (MMS) spacecraft observed an EDR of near-antiparallel magnetopause reconnection on 16 October 2015. An X-type magnetic field configuration and quadrupolar Hall fields, consistent with the electron inflow and outflow, are successfully recovered. While MMS encountered a region of significant energy dissipation on the magnetospheric side of the sub-ion-scale current sheet, the reconstructions show that the MMS tetrahedron missed the X line by a distance of a few kilometers (~2 electron inertial lengths). The estimated reconnection electric field is 0.42–0.98 mV/m, equivalent to the dimensionless reconnection rate of 0.11–0.25. Signatures of three-dimensional structures and/or time-dependent processes are also identified.

Plain Language Summary Magnetic reconnection that often occurs at the outer boundary of Earth's magnetosphere plays a central role in transporting mass and energy of solar wind into the near-Earth space and thus forms the basis of most space weather phenomena, including aurora and geomagnetic storms. However, we still do not fully understand how and how efficiently this process works. We present a two-dimensional image of the magnetic reconnection region reconstructed for the first time from a new data analysis tool by use of high time resolution (30 ms) magnetic field and plasma measurements made by the four-spacecraft Magnetospheric Multiscale (MMS) mission launched in March 2015. The magnetic field configuration and electron velocity field pattern recovered from the tool are consistent with fast magnetic reconnection. But the results show that the MMS spacecraft in fact missed the very site of the reconnection by a distance of a few kilometers (~2 electron inertial lengths) in the event on 16 October 2015 reported by Burch et al. (2016). The results also demonstrate that the new tool is powerful in revealing the structure and fundamental processes of magnetic reconnection in space on the basis of in situ observations.

1. Introduction

The Magnetospheric Multiscale (MMS) mission, four identical spacecraft launched in March 2015, aims at elucidating kinetic processes that are responsible for breaking and reconnecting magnetic field lines in the magnetic reconnection region [*Burch et al.*, 2016a]. MMS has successfully detected the dissipation region of magnetopause reconnection under near-antiparallel field conditions on 16 October 2015 [*Burch et al.*, 2016b]. This region had features that were expected for an electron diffusion region (EDR): an intense electric

current, reversals of the electron jets, dissipation of magnetic energy, crescent-shaped electron velocity distributions carrying the intense current [*Hesse et al.*, 2014], and electron heating along the magnetic field lines.

Sonnerup et al. [2016, hereafter referred to as SEA16] have recently developed a data analysis tool for the reconstruction of steady, two-dimensional (2-D) magnetic field and electron flow in and around the EDR of antiparallel reconnection. The method is based on electron magnetohydrodynamic (EMHD) equations and is an extension of the MHD- and Hall MHD-based reconstruction techniques, an overview of which was given by *Sonnerup et al.* [2008] and *Sonnerup and Teh* [2009]. They help us to understand what type of structure an observing spacecraft encountered and at what time, by providing 2-D maps of the magnetic and/or velocity fields. When data from more than one spacecraft are available, the methods can also be used to estimate the orientation, e.g., of a magnetic flux rope axis, along which spatial gradients may be neglected [e.g., *Hasegawa et al.*, 2006].

In this paper, we report first results from the simplest version of the EMHD reconstruction in which electron inertia is neglected. The method is applied to the event of magnetopause reconnection observed by MMS on 16 October 2015 at ~1307 UT and studied by *Burch et al.* [2016b], *Torbert et al.* [2016], and *Denton et al.* [2016a, 2016b]. The primary objective of the present study is to test the technique using real data, but we also discuss, based on the reconstruction results, the structure of the observed EDR, reconnection rate, and validity of the model assumptions. In section 2, the MMS observations of the reconnection event are briefly summarized. In section 3, we describe essentials of the EMHD reconstruction method. The results are presented in section 4, and a summary and discussion is given in section 5.

2. Overview of the Event

Figure 1 shows burst-mode observations of the magnetic field by the fluxgate magnetometers (FGM) [*Russell et al.*, 2016] and ion and electron moments by the fast plasma investigation (FPI) instruments [*Pollock et al.*, 2016] on board the four MMS spacecraft for a 5 s interval covering the outbound crossing of the postnoon, Southern Hemisphere, magnetopause at 1307:02 UT. Ion and electron data have time resolutions of 150 ms and 30 ms, respectively, and the field data are averaged over 30 ms. The four spacecraft were located at (8.3, 7.1, −4.8) R_E in GSM with separation ~14 km. The LMN axes used here were estimated by *Denton et al.* [2016a, hereafter referred to as DEA16] using a multispacecraft method that we call Maximum Directional Derivative (MDD) analysis [*Shi et al.*, 2005] combined with maximum variance analysis of the magnetic field (MVAB) [*Sonnerup and Scheible*, 1998]. The velocities are shown in the X line rest frame whose velocity (in GSM) is $\mathbf{V}_D = (-47.8, -53.7, -68.6)$ km/s, found using results in DEA16. The guide magnetic field (roughly the B_M component) near and along the X line was rather weak (about −2.5 nT) [*Denton et al.*, 2016b], with the shear angle between the magnetospheric and magnetosheath fields being ~170° [*Burch et al.*, 2016b].

Prominent features of this EDR traversal are an intense current density of ~1.3 $\mu A/m^2$ along the $-M$ direction (Figure 1d) which is mostly supported by electron flows (~1000 km/s) in the $+M$ direction (Figure 1h), southward to northward reversal in both the ion and electron flows (Figure 1g), and positive to negative variation of B_N (Figure 1c). The latter two features suggest that MMS traversed the reconnection region from its southern to northern side. This interpretation is supported by the observed somewhat quadrupolar variations of the Hall magnetic field component B_M [*Denton et al.*, 2016b]. While the density changed by a factor of 5–10 during the entire crossing, it changed only by a factor of 2 for the interval shown in Figure 1. This moderate asymmetry might explain why the quadrupolar, rather than bipolar, Hall field signatures were observed (bipolar B_M signatures are expected for highly asymmetric reconnection [e.g., *Nakamura and Scholer*, 2000]). The B_L, density, and electron velocity oscillations of time scale ~0.5 s observed before the traversal may be due to the structure motion normal to the current sheet (DEA16). As input to the reconstruction, we use the MMS4 data taken during a 0.6 s interval 1307:02.06–1307:02.66 UT between the two dashed lines in Figure 1.

3. Method

The EMHD reconstruction used here assumes a steady, 2-D (i.e., $\partial/\partial t = 0$, $\partial/\partial z = 0$) reconnection geometry in the vicinity of the EDR where ion dynamics is negligible, uniform electron density and temperature ($n = \text{const.}$, $T_e = \text{const.}$), and that electron inertia terms can be neglected. The x axis is antiparallel to the

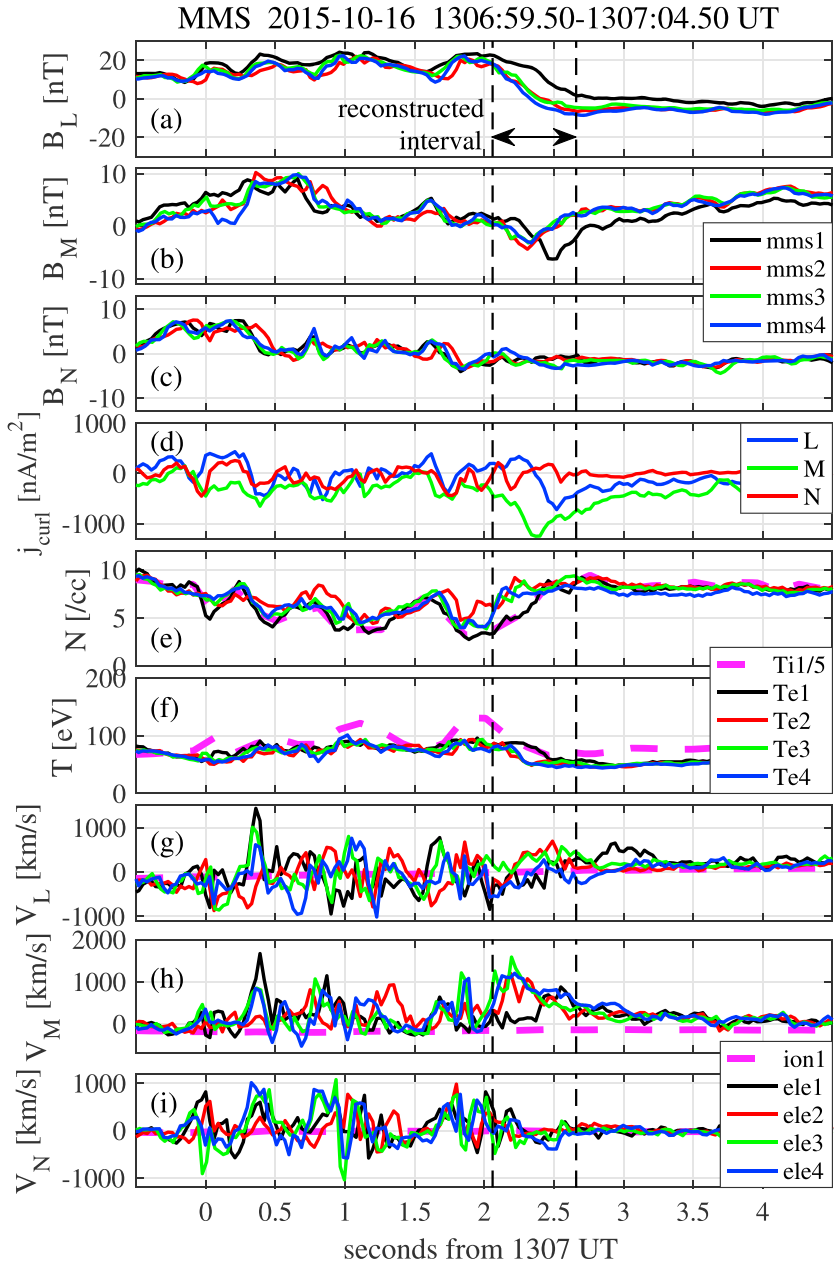

Figure 1. MMS observations in LMN coordinates of (a–c) the magnetic field, (d) electric current estimated by the curlometer technique [*Dunlop et al.*, 2002], (e) density, (f) temperature, and (g–i) velocity when MMS traversed a magnetic reconnection region at the magnetopause. The dashed magenta lines show ion data, and ion temperature is divided by 5 in Figure 1f. The velocities are shown in the structure-rest frame estimated by *Denton et al.* [2016a]. The interval between the two vertical dashed lines is used for the reconstruction. The LMN axes, taken from *Denton et al.* [2016a], are $\mathbf{e}_{LD} = (0.311, 0.488, 0.816)$, $\mathbf{e}_{MD} = (0.481, -0.821, 0.307)$, and $\mathbf{e}_{ND} = (0.819, 0.296, -0.490)$ in GSM.

projection of the velocity $\mathbf{V}_{str}$ of the structure (i.e., the X line rest frame) onto the plane perpendicular to $\hat{\mathbf{z}}$, and the y axis completes the right-handed orthogonal system. The magnetic field and electron velocity are then expressed as $\mathbf{B} = \nabla A \times \hat{\mathbf{z}} + B_z(x,y)\hat{\mathbf{z}}$ and $\mathbf{v} = \nabla\psi \times \hat{\mathbf{z}} + v_z(x,y)\hat{\mathbf{z}}$, respectively, where A is the z component of the vector potential and ψ is the electron stream function. The axial field component B_z is directly related to ψ via $B_z = -\mu_0 ne\psi$. With no electron inertia, the electron momentum equation (i.e., the generalized Ohm's law) becomes

$$\nabla\cdot\mathbf{P} = -ne(\mathbf{E}+\mathbf{v}\times\mathbf{B}), \tag{1}$$

and the axial component v_z of the electron velocity becomes a function of A alone. The transverse field lines are then expressed by the solution of a Grad-Shafranov-like (GS-like) equation

$$\nabla^2 A = -\mu_0 j_Z(A) = \mu_0 n e v_z(A). \tag{2}$$

The simplicity gained in the inertialess version is that the spatial integration of (2) for A is decoupled from that for ψ (i.e., B_z). The reconstructed magnetic potential $A(x,y)$ is thus unaffected by the form of the dissipation term that is responsible for the axial (i.e., reconnection) electric field in the EDR (see the next paragraph). Note also that the reconstruction itself requires as input only the magnetic field and electron moments data from a single spacecraft. Since the ion fluid is assumed to be stationary, electron velocities measured in the ion-rest frame are used to set the initial conditions. See SEA16 or *Hau and Sonnerup* [1999] for details of the actual reconstruction procedure using the GS-like or GS equation and of benchmark tests by use of analytical solution and/or simulation data.

We assume the electron pressure tensor term to be of the form $\nabla\cdot\mathbf{P} = \nabla\widetilde{p}(x,y) + f(x,y)\hat{\mathbf{z}}$, where the in-plane pressure $\widetilde{p}$ is constant under the uniform density and temperature assumption and hence $\nabla\widetilde{p}(x,y) = 0$. As an expression for $f(x,y)$, we adopt the dissipation term for antiparallel reconnection, described in detail by *Hesse et al.* [2011], whose role is equivalent to nongyrotropic electron pressure effects at the X point,

$$f\left(x',y'\right) = n\left(\partial v_{x'}/\partial x'\right)\sqrt{2m_e k_B T_e}. \tag{3}$$

Here the coordinate system (x',y') lies in the xy plane, with the x' axis being parallel to the local tangent to the current sheet. Equation (3) is used to solve the axial component of Ohm's law (1) for $B_z(x,y)$ (i.e., equation (18) in SEA16). Also, equation (25) in SEA16 is used to obtain the 2-D map of electric potential. We thus can produce 2-D maps of the magnetic field, electron velocity, and the potential without use of electric field data.

The reconstruction should be implemented in a proper coordinate system, which is defined after determination of $\mathbf{V}_{\rm str}$ and the $\hat{\mathbf{z}}$ orientation. The initial frame velocity and axis are defined based on $\mathbf{V}_D$ and the M direction $\mathbf{e}_{MD}$, respectively, found by applying the multispacecraft techniques developed by *Shi et al.* [2005, 2006] to four spacecraft measurements of the magnetic field (DEA16). The structure velocity and axial orientation are then optimized by maximizing the correlation coefficient between three GSM components of the magnetic fields and electron velocities predicted from the 2-D field maps at points along the paths of three spacecraft not used as input to the reconstruction and those actually measured, in a way similar to that adopted by *Hasegawa et al.* [2004]. See the supporting information for details of how the coordinate system is optimized. In section 4, we show only results from the MMS4-based reconstruction because the correlation coefficient is highest among the four reconstructions using individual spacecraft, implying that the magnetic and velocity fields are best recovered. See supporting information for the results from the other three spacecraft.

In the steady 2-D geometry, the reconnection electric field E_0 should be constant in space and time (see equation (18) in SEA16). In the reconstruction presented in section 4, we use the median of the axial component of the measured electron convection electric field ($-\mathbf{v}\times\mathbf{B}$), evaluated in the structure-rest frame, as its initial value and then optimize E_0 (see supporting information).

4. Results

Figures 2a–2c show the initial conditions in the reconstruction coordinate system set at $y = 0$ and based on the MMS4 data. The structure velocity (in GSM) is optimized to be $\mathbf{V}_{\rm str} = (-136.5, 30, 1, -162.5)$ km/s, which is larger than the velocity of DEA16. The magnetic field and electron velocity are normalized to the maximum in-plane field component $B_0 = 17.5$ nT and $V_{Ae}/\sqrt{\beta_e}$, respectively. Here the electron Alfvén speed $V_{Ae} = 5.72\times10^3$ km/s and electron beta $\beta_e = 0.815$ are based on the maximum density and pressure values in Figure 2c of $n_0 = 8.39$ cm^{-3} and $p_{e0} = 0.102$ nPa, respectively.

Figure 2d shows B_z and the y component v_y of the normalized electron velocity integrated along the x axis as a function of v_z. Ampère's law requires that these two quantities exhibit strictly the same pattern (but with

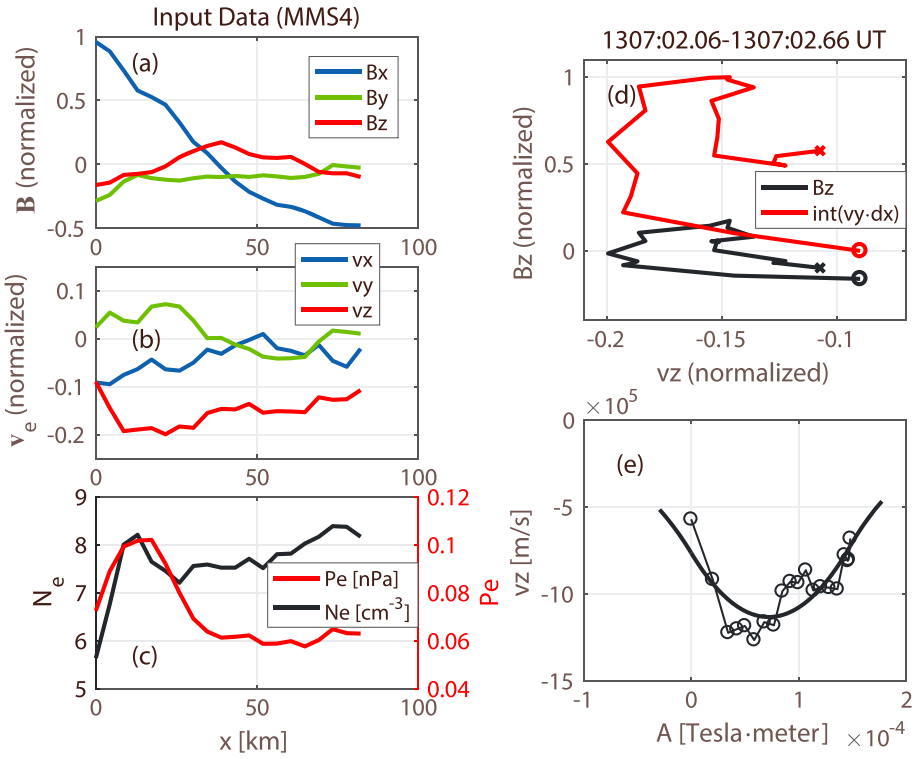

Figure 2. (a) Magnetic field and (b) electron velocity in the reconstruction coordinate system, and (c) electron density and pressure input into the reconstruction using MMS4 data. (d) The axial magnetic field component B_z and the y component of the normalized electron velocity v_y integrated along the x axis versus v_z, which should look similar to each other under the model assumptions. Circles and crosses mark the start and end, respectively, of the data points. (e) The axial electron velocity component v_z versus A. The bold curve shows polynomial function fit to the data. The GSM components of the reconstruction axes are: $\hat{\mathbf{x}}$ = (0.4559, 0.6364, 0.6222), $\hat{\mathbf{y}}$ = (0.7701, 0.0684, −0.6342), and $\hat{\mathbf{z}}$ = (−0.4462, 0.7683, −0.4589).

offset) under the model assumptions of 2-D, time independence, uniform number density, constant structure velocity, and negligible ion current. The discrepancy seen in Figure 2d (and also for the other spacecraft) implies that some or all of the above assumptions are violated in this event. Here we use B_z, rather than the integrated v_y, to set the initial condition at $y = 0$ for the B_z (i.e., ψ) integration, because we judge the measurements of the magnetic field to be more reliable than those of the electron moments.

Figure 2e shows that v_z as a function of partial vector potential A (i.e., $-B_y$ integrated along the x axis) can be expressed by a single curve. This is because in this particular case B_y happens to be negative throughout the interval (Figure 2a), and thus, A monotonically increases along the x axis. However, it is likely that other cases may exhibit a double-branch feature (see, e.g., Figure 5b in SEA16) and, in a future study, finite electron inertia effects must be taken into account to allow for v_z being variable along the transverse field lines.

Figure 3 shows the magnetic field and electron streamline maps reconstructed from the MMS4 data. The electron current density (i.e., v_z) is preserved along the transverse field lines (Figure 3a), as required for the incompressible EMHD system without electron inertia, and B_z is constant along the electron streamlines (Figure 3b) because $B_z = -\mu_0 ne\psi$. Figure 3a demonstrates that an X-type field geometry expected at the reconnection site is successfully recovered, and the current sheet thickness near the X point (marked as a cross) is comparable to the electron inertial length (~2 km). Number "2" and letter "D" in Figure 3a denote the locations of the X point reconstructed from MMS2 data and that estimated by DEA16, respectively. Maps with the correlation coefficients higher than 0.1 were not obtained from MMS1 data, possibly because MMS1 was farthest from the X point among the four spacecraft. Also, the MMS3 reconstruction for an interval 1307:02.04–1307:02.64 UT shows that the X point is not within, but slightly to the left (southward) of, the reconstruction domain (Figure S2). Nevertheless, all the results suggest that MMS4 made the

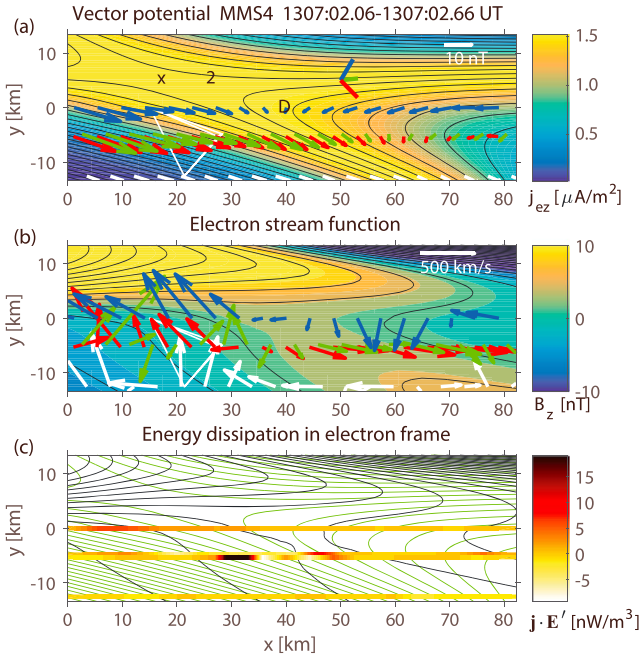

Figure 3. (a) Transverse magnetic field lines reconstructed from MMS4 data with the axial electron current in color. The blue, green, and red bars at upper right are projections onto the *xy* plane of the GSM *x*, *y*, and *z* axes (the magnetosheath is at the top, and the magnetosphere is at the bottom). See text for what marks "cross", "D", and "2" mean. (b) Reconstructed in-plane electron streamlines with the axial field component in color. The arrows in Figures 3a and 3b show the measured magnetic field and electron velocity vectors in the structure-rest frame, respectively, from the four spacecraft (MMS1: white, MMS2: red, MMS3: green, MMS4: blue). (c) Scalar product of current density and electric field in the electron-rest frame, as a measure of energy dissipation, measured along the paths of the four spacecraft. MMS moved from left to right in the maps. Green lines show the reconstructed field lines, while black lines show the electron streamlines. In reconstruction coordinates, MMS1, MMS2, and MMS3 are at $z = 1.1$, 7.1, and -6.4 km, respectively.

closest approach to the X-point at ~1307:02.2 UT and, even then, the MMS tetrahedron did not encounter, but was at a few kilometers earthward of, the X line.

The opening angle of the separatrix field lines, defined here as the angle between the average directions of the magnetosheath and magnetospheric field lines passing through the X point, is found to be ~23° (see supporting information for how the opening angle is estimated). This is comparable to that (~28°) expected for the dimensionless reconnection rate of ~0.25, estimated from the constant reconnection electric field $E_0 = 0.98$ mV/m used in the reconstruction.

Figure 3b show that the electron inflow and outflow pattern expected in the reconnection region is qualitatively recovered. However, the stagnation point at $(x, y) \sim (45, -5)$ km is displaced northward and to the magnetospheric side of the X point, and B_z errors appear to be large (dark blue color) near the upper right corner. The shift of the stagnation point toward the magnetosphere is a characteristic of asymmetric reconnection [*Hesse et al.*, 2014] and is consistent with the earlier report that the dissipation region is displaced to the magnetospheric side [*Burch et al.*, 2016b]. The measured electron velocity vectors are not parallel to the recovered streamlines in many places on the spacecraft paths. Possible sources of this discrepancy will be discussed in section 5 and should be pursued in the future. Nevertheless, we recovered a somewhat quadrupolar Hall magnetic field pattern, as revealed by DEA16 for this event. The axial field B_z near the X point is positive (i.e., B_M is negative), consistent with the weak guide field component present in this event, as confirmed by *Denton et al.* [2016b]. Note that even the electron velocities from MMS4 (blue arrows at $y = 0$) are not always tangential to the streamlines. This is due to our choice that the measured axial field B_z, rather than ψ (i.e., measured v_y integrated along the x axis), is used when initiating the reconstruction.

Figure 4 shows a comparison of the three components of the measured magnetic fields and the electron velocities in the structure-rest frame and those predicted from the maps along the paths of the three spacecraft not used in the MMS4 reconstruction. The bootstrap method is used to estimate the confidence interval of the correlation coefficients [e.g., *Kawano and Higuchi*, 1995]. It is remarkable that the timing of the rapid B_L decrease and larger $|B_M|$ value at 1307:02.5 UT seen by MMS1, which is farthest from MMS4 in the *xy* plane (Figure 3), are well recovered by the reconstruction. The correlation coefficient is significantly higher for the magnetic field (cc = 0.976) than for the electron velocity (cc = 0.888) in all four reconstructions using individual spacecraft (see supporting information). Possible reasons for this difference will be discussed in section 5. We note that the two correlation coefficients are both higher than those obtained by assuming that the predicted values are the same as what MMS4 measured (cc = 0.793 for the magnetic field and cc = 0.851

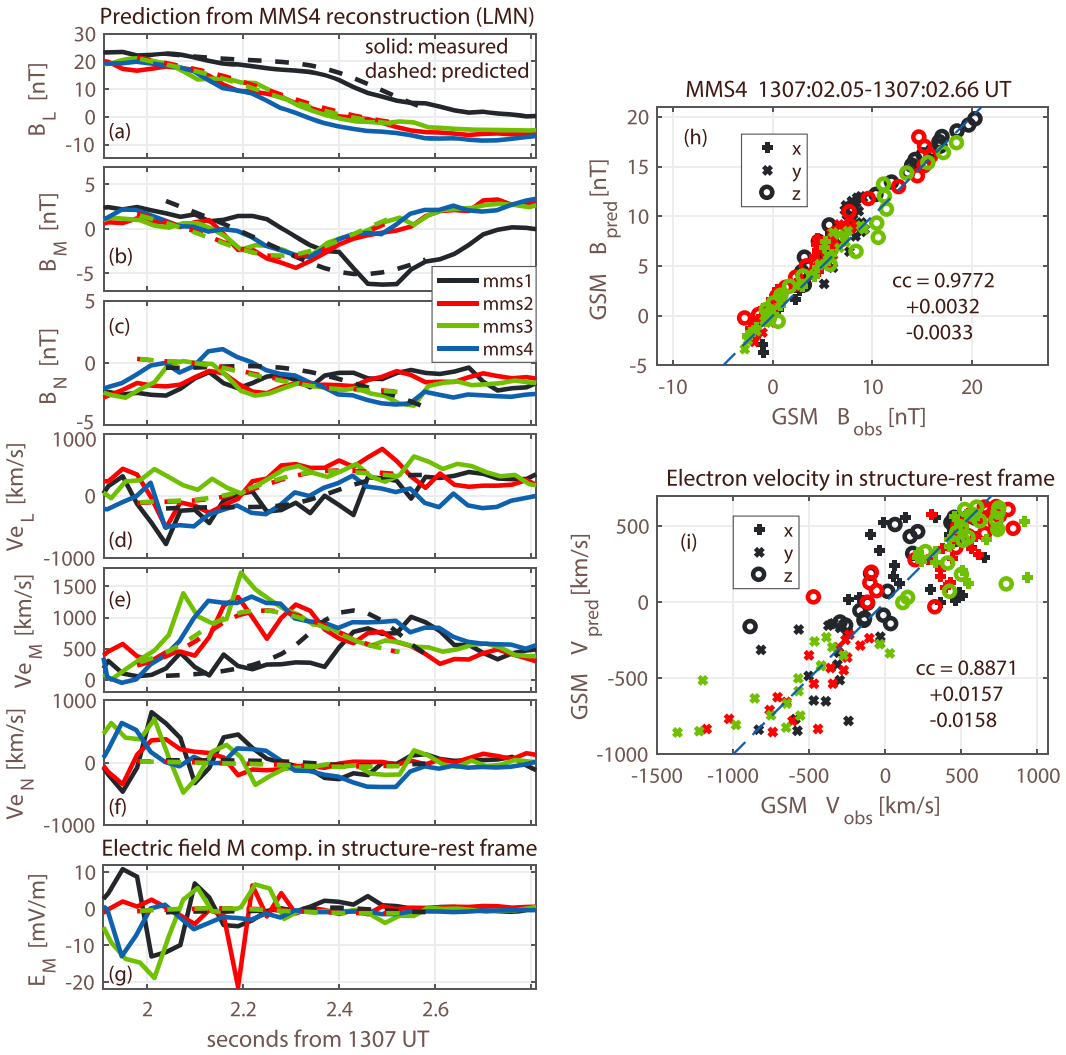

Figure 4. (a–g) Time series of the measured magnetic fields and electron velocities in LMN and the *M* component of the electric fields in the structure-rest frame and those predicted along the paths of the three spacecraft not used in the reconstruction. (h, i) Correlation plots of the measured and predicted components in GSM, along with the confidence intervals of the correlation coefficient corresponding to ±1 sigma. The electric fields were measured by the spin-plane and axial double probes (SDP and ADP) (Figure 4g) [*Lindqvist et al.*, 2016; *Ergun et al.*, 2016].

for the electron velocity). This indicates that the observed variations, including current sheet crossing and electron jet reversal, are generally well recovered by the reconstruction.

Figure 3c shows a proxy of energy dissipation $\mathbf{j}\cdot\mathbf{E}' = \mathbf{j}\cdot(\mathbf{E}+\mathbf{v}\times\mathbf{B})$ [*Zenitani et al.*, 2011] measured along the paths of the four spacecraft, as a demonstration of how the reconstruction results could be used for better data interpretation. Current densities based on the ion and electron moments and 30 ms averages of the double probe electric field measurements [*Ergun et al.*, 2016; *Lindqvist et al.*, 2016] are used here. Significant dissipation is seen near, but on the magnetospheric side of, the X point, consistent with the results reported earlier [*Burch et al.*, 2016b; *Torbert et al.*, 2016; DEA16]. Since the constant reconnection electric field used in the reconstruction is $E_0 = 0.98$ mV/m and the axial current density around the X point is of order 1 μA/m^2 (Figure 3a), the energy dissipation rate expected for steady 2-D reconnection is of order 1 nW/m^3. Thus, the peaks in the dissipation proxy $\gtrsim$10 nW/m^3 on the MMS2 and MMS3 paths are probably not directly associated with reconnection but due to some 3-D or wave effects, as discussed by *Fujimoto and Sydora* [2012] and *Price et al.* [2016]. Indeed, highly variable E_M predominantly on the magnetospheric side (Figure 4g) may be an indication of such 3-D or nonsteady processes.

5. Summary and Discussion

We have successfully recovered the EDR of nearly antiparallel magnetopause reconnection reported by *Burch et al.* [2016b] by use of the 2-D, incompressible, inertialess version of EMHD reconstruction based on the dissipation term described by *Hesse et al.* [2011]. All four reconstructions using individual spacecraft show that the MMS tetrahedron did not encounter but was a few kilometers away from the X line even at the closest approach, while MMS passed through the region of significant energy dissipation located on the magnetospheric side of the X line [*Burch et al.*, 2016b]. We note that simulation studies show that the region of maximum dissipation $\mathbf{j}\cdot\mathbf{E}'$ is shifted toward the magnetosphere for asymmetric reconnection, as in the present magnetopause event [*Zenitani et al.*, 2011; *Torbert et al.*, 2016].

It is obvious from comparison between the measured magnetic and velocity fields and those predicted from the maps (Figure 4) that the electron velocities are less well recovered than the magnetic fields. Indeed, the locations of the electron flow stagnation point are considerably different among the four reconstructions (see supporting information). Neglecting electron inertia and the specific form of the dissipation term used here may be the factors responsible for this difference, in addition to 3-D and time-dependent effects and less accurate measurements of electron moments than the magnetic field. We note that in the benchmark test of the inertialess EMHD reconstruction using a 2-D PIC simulation, the errors are generally larger for ψ than A (Figure 6 in SEA16). Moreover, 2-D simulations of asymmetric reconnection show that electron nongyrotropy is a major contributor to the reconnection electric field at the stagnation point, but not at the X point, i.e., inertia effects play an important role at the X point [*Hesse et al.*, 2014]. It is also likely that the axial component of the current density is not preserved along the transverse field lines as assumed in the present inertialess reconstruction but has a maximum near the X point. The next step necessary for the method improvement is thus to include inertia effects, which is currently under way. We believe, however, that the present method would work better for near-symmetric magnetotail reconnection to be observed during Phase 2 of the MMS mission than in the case reported here.

We note that the invariant axis optimized for the MMS4 reconstruction (Figure 3) has an angle of 9.4° with $-\mathbf{e}_{MD}$, estimated by DEA16 using the combined MDD-MVAB method, which is much smaller than the angle of 22.7° with $-\mathbf{e}_{MB}$, the $-M$ axis used by *Burch et al.* [2016b] for a different interval. Their $\mathbf{e}_{MB}$ was defined to be the intermediate magnetic variance direction, and its GSM components are (0.5694, −0.8173, 0.0886). The result suggests that at least for this event, the MDD-MVAB method provides a more accurate estimate of the invariant axis or X-line orientation than does MVAB on its own.

As a result of the coordinate system optimization, we can obtain the value of the constant reconnection electric field E_0 under the assumption of 2-D steady reconnection. For the four reconstructions, it ranges between 0.4 and 1.0 mV/m, equivalent to the dimensionless reconnection rate of 0.11–0.25 (Table S1 in the supporting information). While these estimates are reasonable, significant E_0 differences among the three reconstructions and other signatures (Figures 2d and 4g) indicate that 3-D and/or time-dependent processes were involved in the observed magnetopause reconnection. DEA16 indeed found that the intermediate magnetic gradient direction was closer to the M than to the L direction, suggesting some structures in the X line direction. Note also that although MMS2 and MMS3 traversed similar regions of the 2-D maps nearly at the same time (Figure 3), the X point location is different between the two reconstructions (see supporting information). These features suggest the presence of nonnegligible inhomogeneity along the X line direction (MMS2 and MMS3 were separated by ~14 km in the z direction). Revealing such aspects remains as a future task.

Acknowledgments
MMS data are available from the MMS Science Data Center: https://lasp.colorado.edu/mms/sdc/public/. The MATLAB code for the reconstruction is available upon request to H.H. The work by H.H. was supported by JSPS Grant-in-Aid for Scientific Research KAKENHI 15K05306. Work at Dartmouth was supported by NASA grant NNX14AC38G.

References

Burch, J. L., T. E. Moore, R. B. Torbert, and B. L. Giles (2016a), Magnetospheric Multiscale overview and science objectives, *Space Sci. Rev.*, *199*, 5–21, doi:10.1007/s11214-015-0164-9.

Burch, J. L., et al. (2016b), Electron-scale measurements of magnetic reconnection in space, *Science*, *352*, aaf2939, doi:10.1126/science.aaf2939.

Denton, R. E., B. U. Ö. Sonnerup, H. Hasegawa, T.-D. Phan, C. Russel, R. J. Strangeway, B. L. Giles, D. J. Gershman, and R. B. Torbert (2016a), Motion of the MMS spacecraft relative to the magnetic reconnection structure observed on 16 Oct 2015 at 1307 UT, *Geophys. Res. Lett.*, *43*, 5589–5596, doi:10.1002/2016GL069214.

Denton, R. E., B. U. Ö. Sonnerup, H. Hasegawa, T.-D. Phan, C. T. Russell, R. J. Strangeway, B. L. Giles, and R. B. Torbert (2016b), Reconnection guide field and quadrupolar structure observed by MMS on 16 Oct 2015 at 1307 UT, *J. Geophys. Res. Space Physics*, *121*, 9880–9887, doi:10.1002/2016JA023323.

Dunlop, M. W., A. Balogh, K.-H. Glassmeier, and P. Robert (2002), Four-point Cluster application of magnetic field analysis tools: The Curlometer, *J. Geophys. Res.*, *107*(A11), 1384, doi:10.1029/2001JA005088.

Ergun, R. E., et al. (2016), The axial double probe and fields signal processing for the MMS mission, *Space Sci. Rev.*, *199*, 167–188, doi:10.1007/s11214-014-0115-x.

Fujimoto, K., and R. Sydora (2012), Plasmoid-induced turbulence in collisionless magnetic reconnection, *Phys. Rev. Lett.*, *109*, 265004, doi:10.1103/PhysRevLett.109.265004.

Hasegawa, H., B. U. Ö. Sonnerup, M. W. Dunlop, A. Balogh, S. E. Haaland, B. Klecker, G. Paschmann, I. Dandouras, B. Lavraud, and H. Rème (2004), Reconstruction of two-dimensional magnetopause structures from Cluster observations: Verification of method, *Ann. Geophys.*, *22*, 1251–1266, doi:10.5194/angeo-22-1251-2004.

Hasegawa, H., B. U. Ö. Sonnerup, C. J. Owen, B. Klecker, G. Paschmann, A. Balogh, and H. Rème (2006), The structure of flux transfer events recovered from Cluster data, *Ann. Geophys.*, *24*, 603–618, doi:10.5194/angeo-24-603-2006.

Hau, L.-N., and B. U. Ö. Sonnerup (1999), Two-dimensional coherent structures in the magnetopause: Recovery of static equilibria from single-spacecraft data, *J. Geophys. Res.*, *104*(A4), 6899–6917, doi:10.1029/1999JA900002.

Hesse, M., T. Neukirch, K. Schindler, M. Kuznetsova, and S. Zenitani (2011), The diffusion region in collisionless magnetic reconnection, *Space Sci. Rev.*, *160*, 3–23, doi:10.1007/s11214-010-9740-1.

Hesse, M., N. Aunai, D. Sibeck, and J. Birn (2014), On the electron diffusion region in planar, asymmetric, systems, *Geophys. Res. Lett.*, *41*, 8673–8680, doi:10.1002/2014GL061586.

Kawano, H., and T. Higuchi (1995), The bootstrap method in space physics: Error estimation for minimum variance analysis, *Geophys. Res. Lett.*, *22*, 307–310, doi:10.1029/94GL02969.

Lindqvist, P.-A., et al. (2016), The Spin-plane Double Probe electric field instrument for MMS, *Space Sci. Rev.*, *199*, 137–165.

Nakamura, M. S., and M. Scholer (2000), Structure of the magnetopause reconnection layer and of flux transfer events: Ion kinetic effects, *J. Geophys. Res.*, *105*(A10), 23,179–23,191, doi:10.1029/2000JA900101.

Pollock, C., et al. (2016), Fast plasma investigation for Magnetospheric Multiscale, *Space Sci. Rev.*, *199*, 331–406, doi:10.1007/s11214-016-0245-4.

Price, L., M. Swisdak, J. F. Drake, P. A. Cassak, J. T. Dahlin, and R. E. Ergun (2016), The effects of turbulence on three-dimensional magnetic reconnection at the magnetopause, *Geophys. Res. Lett.*, *43*, 6020–6027, doi:10.1002/2016GL069578.

Russell, C. T., et al. (2016), The Magnetospheric Multiscale magnetometers, *Space Sci. Rev.*, *199*, doi:10.1007/s11214-014-0057-3.

Shi, Q. Q., C. Shen, Z. Y. Pu, M. W. Dunlop, Q.-G. Zong, H. Zhang, C. J. Xiao, Z. X. Liu, and A. Balogh (2005), Dimensional analysis of observed structures using multipoint magnetic field measurements: Application to Cluster, *Geophys. Res. Lett.*, *32*, L12105, doi:10.1029/2005GL022454.

Shi, Q. Q., C. Shen, M. W. Dunlop, Z. Y. Pu, Q.-G. Zong, Z.-X. Liu, E. A. Lucek, and A. Balogh (2006), Motion of observed structures calculated from multi-point magnetic field measurements: Application to Cluster, *Geophys. Res. Lett.*, *33*, L08109, doi:10.1029/2005GL025073.

Sonnerup, B., and M. Scheible (1998), Minimum and maximum variance analysis, in *Analysis Methods for Multi-Spacecraft Data*, edited by G. Paschmann and P. Daly, pp. 185–220, Int. Space Sci. Inst, Bern, Switzerland.

Sonnerup, B. U. Ö., and W.-L. Teh (2009), Reconstruction of two-dimensional coherent structures in ideal and resistive Hall MHD: The theory, *J. Geophys. Res.*, *114*, A04206, doi:10.1029/2008JA013897.

Sonnerup, B. U. Ö., W.-L. Teh, and H. Hasegawa (2008), Grad-Shafranov and MHD reconstructions, in *Multi-Spacecraft Analysis Methods Revisited*, edited by G. Paschmann and P. W. Daly, pp. 81–90, ESA Publications Division, Bern, Switzerland.

Sonnerup, B. U. Ö., H. Hasegawa, R. E. Denton, and T. K. M. Nakamura (2016), Reconstruction of the electron diffusion region, *J. Geophys. Res. Space Physics*, *121*, 4279–4290, doi:10.1002/2016JA022430.

Torbert, R. B., et al. (2016), Estimates of terms in Ohm's law during an encounter with an electron diffusion region, *Geophys. Res. Lett.*, *43*, 5918–5925, doi:10.1002/2016GL069553.

Zenitani, S., M. Hesse, A. Klimas, and M. Kuznetsova (2011), New measure of the dissipation region in collisionless magnetic reconnection, *Phys. Rev. Lett.*, *106*, 195003, doi:10.1103/PhysRevLett.106.195003.